APPLIED ORGANOMETALLIC CHEMISTRY
Appl. Organometal. Chem. 2007; **21**: 514–520
Published online in Wiley InterScience
(www.interscience.wiley.com) DOI:10.1002/aoc.1272

Alkynylorganotins, versatile precursors of class II hybrid materials

Thierry Toupance*, Mervyn de Borniol, Hicham El Hamzaoui and Bernard Jousseaume

University Bordeaux 1, Institut des Sciences Moléculaires, Groupe Matériaux, UMR 5255 CNRS, 351 Cours de la Libération, F33405 Talence Cedex, France

Received 27 March 2007; Revised 28 March 2007; Accepted 28 March 2007

In the field of functional organic–inorganic hybrid materials, recent trends in the chemistry based on trialkynylorganotins 1 and organically bridged α,ω-bis(trialkynyltin) compounds 2 are reviewed. Compounds 1 reacted with non-porous silica and nanoporous tin dioxide powders to yield hydrophobic, lipophobic or perylene dye-modified oxide materials. The formation of M_{oxide}–O–Sn–C bonds and the release of three molecules of alkyne led to the irreversible chemisorption of 1, the reaction rate and the chain loading depending on the electronic demand and the bulkiness of the organic group grafted. Furthermore, self-assembled tin-based class II hybrid materials were spontaneously formed by hydrolysis of 2 under homogeneous conditions as the two tin atoms were bridged through a rigid or a semi-rigid linker. Subsequent thermal treatment of these hybrids under an oxygen flow at 400–500 °C furnished nanoporous tin dioxide materials consisting of a porous network of aggregated cassiterite tin dioxide particles. An unusual polymodal distribution of mesopore sizes was found in the case of the sample prepared from the hybrid containing the diphenylene spacer.

KEYWORDS: alkynylorganotins; grafting; auto-organization; hybrid materials; tin dioxide

INTRODUCTION

Functional organic–inorganic hybrid materials, which associate in nanosized-level active inorganic and organic or even bioactive components, have attracted a worldwide attention stimulated because of their numerous applications in fields including catalysis, electronics, optoelectonics and medecine.[1] As their local structure and degree of organization govern both their chemical and physical properties, different synthetic methods have been established to design tailor-made hybrid materials. They include the conventional sol–gel route from organofunctional or bridged alkoxides,[2] the assembling of well-defined nanobuilding blocks,[3] template-directed self-assembly procedures in the presence or absence of nanobuilding blocks,[4] integrative approaches which combine the previous methods with micro-molding routes[5] and also the chemical modification of oxide surfaces with an organic functionality.[6] Among these materials, class II hybrid materials, where the organic and inorganic components are linked through strong covalent bonds, occupy a specific place due to their expected high chemical and mechanical stabilities. The preparation of bridged silsesquioxane hybrid materials showing controlled texture and morphology both at the mesoscopic and molecular scales has been successfully achieved by the hydrolysis-condensation of bis-(trialkoxysilyl)alkylene, arylene and benzylene derivatives in the presence of organic templates.[7–9] Moreover, long-range ordered structures were spontaneously formed from similar precursors when the organic bridge between the two silicon centers contained functional groups favoring the self-assembly of the organic component via hydrogen bonding.[10] On the other hand, coupling agents such as chloro-,[11] hydrido-[12] or allylsilanes[13] have been widely used for surface functionalization and modification of oxide particles and films to confer new

*Correspondence to: Thierry Toupance, University Bordeaux 1, Institut des Sciences Moléculaires, Groupe Matériaux, UMR 5255 CNRS, 351 Cours de la Libération, F33405 Talence Cedex, France.
E-mail: t.toupance@ism.u-bordeaux1.fr
Contract/grant sponsor: Aquitaine Region (MdB fellowship).
Contract/grant sponsor: The Centre National de la Recherche Scientifique (Material Program Grant).
Contract/grant sponsor: European Community (FAME Network of Excellence).

properties on them such as water[6] and/or fat[14] repulsion, ion detection[15] and catalyst immobilization.[13] Nonetheless, most of the studies have concerned silica-based materials and little attention has been paid to the development of a similar approach for transition or main group metal-based hybrid materials, probably due to a too narrow range of precursors available. In particular, very few examples of tin-based hybrids have been described so far despite the unique physical properties of tin dioxide materials, i.e. electronic conductivity and optical transparency along with high mechanical and chemical stabilities. The main example involves the assembly of tin–oxo hydoxo clusters using telechelic organic biscarboxylic acid derivatives.[16,17] To draw new prospects in this field, we have developped original synthetic routes towards hydrolysable organotins for sol–gel chemistry and chemical modification of oxide surfaces since tin is one of the rare metals that form stable metal–carbon bonds under hydrolytic conditions. In this context, functional trialkynylorganotins[18,19] and organically bridged α,ω-bis(trialkynyltin) compounds[20,21] have been synthesized, which afforded surface modified oxides[19,22] and self-assembled tin-based hybrid materials[23–25] after reaction with oxide powders or films and controlled hydrolysis, respectively. Alkynylorganotins appeared to be very suitable precursors for different fundamental and practical reasons: (i) the alkynyl functionality is removed upon hydrolysis as an inert gas or liquid, which prevents any pollution or decomposition of the resulting hybrids; (ii) their hydrolysis rate lies between the chloride and alkoxide ones favoring the formation of gels; (iii) their reaction with hydroxylated species can be easily monitored by IR spectroscopy.

We herein present a review of some aspects of the chemistry based on alkynylorganotins **1** and **2** (Scheme 1). The reactivity of the trialkynylorganotins towards oxide materials will be related to the steric hindrance of the chain grafted and one application of the hybrid obtained will be mentioned. Furthermore, an overview of the nano-organization in tin-based hybrid materials prepared from **2** will be presented along with the texture, structure and morphology of the tin dioxide materials obtained after calcination.

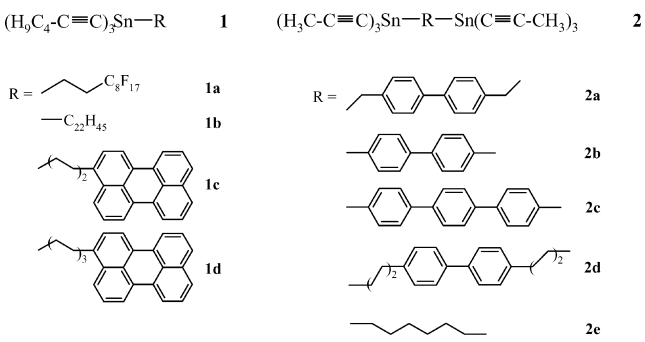

Scheme 1. Chemical formula of precursors **1** and **2**.

MATERIALS AND METHODS

Tetrahydrofuran was distilled over Na/benzophenone prior to use. Elemental analyses were carried out by the 'Service Central d'Analyse du CNRS' in Vernaison, France. Organotins **1** and **2** were synthesized as previously described.[18–21,24] Grafting experiments have been done according to published procedures.[19,22] Hydrolysis experiments were conducted as follows. In a Schlenk tube, a mixture of water (350 mmol), HCl (1 M, 0.63 mmol) and THF (300 mmol) were added dropwise to a solution of **2** (4.6 mmol) in THF (300 mmol). After stirring for 10 min, the reaction mixture was stood at room temperature. The gel transition occurred within 2 or 3 weeks. The solvent was then removed under reduced pressure and the crude materials were washed with THF to eliminate undesirable organics. The resulting powder was finally dried *in vacuo* at 120 °C for 3 h to furnish pale yellow xerogels. In the following, the samples are labeled X_p^T where p and T stand for the precursor label and the temperature of the thermal treatment, respectively. The chemical composition of xerogels $\mathbf{X_{2a}}^{120}$ and $\mathbf{X_{2d}}^{120}$ has been reported previously.[23,24]

Elemental analysis: calculated for $\mathbf{X_{2b}}^{120}$: $Sn_2(C_{12}H_8)_1O_2(OH)_2$: Sn, 52.1; O, 14.1; C, 31.6; H, 2.2; found: Sn, 53.1; O, 13.9; C, 30.0; H, 2.9. $\mathbf{X_{2c}}^{120}$: $Sn_2(C_{18}H_{12})_1O_2(OH)_2.1H_2O$: Sn, 43.1; O, 14.5; C, 39.36; H, 2.9; found: Sn, 43.1; O, 14.7; C, 39.0; H, 3.1. $\mathbf{X_{2e}}^{120}$: $Sn_2(C_6H_{12})_1O_3$: Sn, 64.2; O,13.0; C, 19.5; H, 3.3; found: Sn, 62.9; O, 13.8; C, 19.7; H, 3.6.

Hybrid xerogels $\mathbf{X_{2b}}^{120}$ and $\mathbf{X_{2e}}^{120}$ were then calcined in an oxygen flow for 4 h at 400 or 500 °C. IR spectra (KBr pellets) were recorded on an FTIR Perkin-Elmer spectrophotometer. TGA-MS measurements were performed on a Netzsch STA 409 simultaneous analyzer coupled with a Thermostar Balzers Instrulents quadrupole spectrometer. The thermogravimetric (TG) curves were obtained in the 25–650 °C temperature range with a heating rate of 5 °C min^{-1} under an argon or air flow. Powder X-ray diffraction patterns were collected with a Philips θ–2θ PW1820 or a Nanostar AXS (Bruker GmbH) diffractometer. Nitrogen adsorption porosimetry was carried out on an ASAP2010 (Micromeritics) apparatus. Specific surface areas were calculated by applying the BET equation between 0.1 and 0.3 relative pressure. Pore size distributions were determined by the Barrett, Joyner, Halenda (BJH) method using the adsorption isotherm branch.[26] TEM images were taken with a Jeol-JEM 100 SX microscope.

RESULTS AND DISCUSSION

Surface functionalization of oxide surfaces

The reactivity of functional trialkynylorganotins towards the surface hydroxyl groups of metal oxide was first demonstrated by reacting precursor **1a** with a nonporous silica powder. The amount of chemisorbed stannane **1a** indeed varied between 0.05 and 0.28 mmol g^{-1}, i.e. 0.3 and 1.7 chain nm^{-2}, in the final materials by a careful tuning of the precursor content in the grafting solution and both reaction

DOI: 10.1002/aoc

Table 1. Loadings of **1a, b** and chain densities on non-porous Biosepra 100 silica (100 $m^2.g^{-1}$) at room temperature

Precursor[a]	Loading (mmol g^{-1})	Chain density (chain nm^{-2})
1a	0.24	1.4
1b	0.34	2.1
$(F_{17}H_4C_{10})SiCl_3$	0.44	2.6

[a] Mole number of precursor introduced: 0.68 $mmol.g^{-1}$.

time and temperature. Reaction of 0.28 mmol g^{-1} of **1a** at room temperature overnight (15–18 h) furnished the denser layer, the final chain loadings remaining constant when a higher starting content in **1a** was used. The formation of a fluorinated chain thin layer, probably a monolayer, was evidenced by elemental microanalysis, FTIR spectroscopy, solid-state CP-MAS NMR, XPS and TGA-MS measurements, irreversible chemisorption of **1a** occuring via the release of the three alkynyl functionalities and the formation of $Si_{bulk}-O-Sn-C$ linkages.[19] Then, the question arose about the influence of the chain nature on the reactivity of the trialkynylorganotins, which led us to conduct similar studies with **1b** (Table 1). First of all, compound **1b** reacted much more slowly than **1a**, the maximum chain loading being reached after more than 5 days. This behavior could be rationalized by considering that the electrondonating long alkyl group made the tin center less electrophilic than the electronwithdrawing fluorinated chain did, which therefore disfavored the nucleophilic attack of hydroxylated species at the tin center. Nonetheless, compound **1b** gave surface modified silicas with alkyl chain loadings as high as 0.34 mmol g^{-1} compared with 0.24 $mmol.g^{-1}$ obtained with **1a** in the same experimental conditions. As expected on the basis of the steric hindrance of both chains, the less bulky one yielded higher chain loadings. More interestingly, the ratio between the alkyl and fluorinated chain contents, ca. 1.5, closely matched the ratio between the cross-sectional area of a perfluorinated chain and an alkyl chain, which have been estimated to be 30 and 20 $Å^2$, respectively. Consequently, these results showed that the chain loading and the reaction time of trialkynylorganotins bearing flexible linear organic groups towards silica were ruled by the electronic demand and the bulkiness of the chain. However, trialkynylorganotins did not allow layers to be obtained as dense as those obtained with organosilanes, such as for instance trichlorofluoroorganosilanes. This was attributed to a slower hydrolysis rate of **1a** which would favor polycondensation reactions in solution and, therefore, would limit surface reactions and self-organization of the chains at the oxide surface.[19]

Organotins **1a** and **1c–d** were also reacted with nanoporous tin dioxide powders to give modified SnO_2 nanohybrids.[22] For instance, the amount of deposited perylene core linearly increased up to a plateau value of 0.13 mmol g^{-1}, i.e. 1.6 chain nm^{-2}, as the amount of **1c–d** in the grafting solution was increased (Fig. 1). As described above, elemental analysis and solution IR measurements confirmed the departure of three molecules of hexyne per perylene core deposited along with the formation of $Sn_{bulk}-O-Sn-C$ bonds. These results were therefore in favor of an irreversible chemisorption of **1**, probably as a monolayer, since the existence of a plateau value from a starting precursor concentration precluded any continuous polycondensation of **1** at the oxide surface. This new functionalization method of metal oxide surfaces found a very promising application in the field of the photosensitization of semiconducting oxide for energy conversion purpose. Measurements carried out on dye-modified SnO_2 nanoporous powders led to a significant photocurrent starting at 0.75 V/SCE under illumination in the presence of an aqueous electrolyte.[27] The methodology was then applied to the surface modification of nanoporous SnO_2 thin films with **1c–d**. Under white light illumination (400–700 nm, 80 mW cm^{-2}), the resulting photoelectrochemical cells showed overall conversion efficiencies ranging from 0.02 to 0.04% with short-circuit current densities (J_{sc}) of 180–240 $mA.cm^{-2}$, open-circuit photovoltages (V_{oc}) of −0.36 V and fill factors of 0.28–0.35.[22] Even though the device performances were quite fair in the field of dye-sensitized solar cells,[28] the approach investigated here was validated by these results.

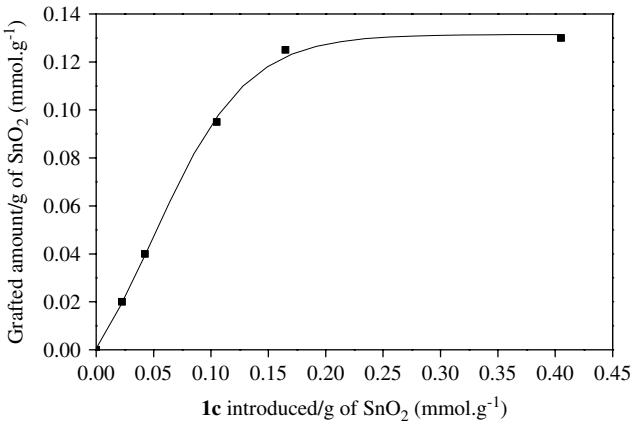

Figure 1. Evolution of the amount of perylene dye deposited as a function of **1c** content in the grafting solution.

In summary, this method based on alkynylorganotins has allowed specific organic functionalities to be added to silica and tin dioxide surfaces, widening the range of the precursors available to design functional hybrid materials. To the best of our knowledge, this work constitutes the first example of grafted organotins on oxide supports obtained by a solution route.

Self-assembled tin-based hybrid materials and mesoporous tin dioxide

Preliminary studies carried out with **2a** have shown that a mixed aromatic–aliphatic linker induces hydrophobic interaction between the spacers strong enough to afford,

DOI: 10.1002/aoc

under standard hydrolysis conditions, self-assembled tin-based hybrid materials in which layers of stacked organic spacers alternate with tin oxide layers.[23] To obtain a better insight into the role of the chemical nature of the linker on the organization of tin-based hybrid materials, the same experiments were repeated with **2b–e**. For example, hydrolysis of precursor **2b** in THF in the presence of HCl as a catalyst yielded the xerogel $\mathbf{X_{2b}}^{120}$ after ageing for several days and subsequent drying at 120 °C. By IR spectroscopy, resonances assigned to the organic spacer were observed at 1589 and 1480 cm^{-1} [$\nu_{ring}(C{=}C) + \nu_{ring}(C{=}C)$], 1076 and 1002 cm^{-1} [$\delta(C_{ring}H$ in-plane)] and 804 cm^{-1} [$\delta(C_{ring}H$ out-of-plane)], along with broad bands between 700 and 500 cm^{-1} indicating the formation of Sn–O–Sn and Sn–OH bonds (Fig. 2). In addition, the disappearance of the features characteristic of the Sn–C≡C group (2169 and 998 cm^{-1}) revealed that each alkynyl functionality has been removed with the concomitant formation of a tin–oxygen band. TGA-MS studies confirmed the presence of the 4,4′-biphenylene linker. The TG of $\mathbf{X_{2b}}^{120}$ in air showed a continuous mass loss between 25 and 650 °C occurring in three successive steps of 5% (from 25 to 111 °C), 20% (from 111 to 272 °C) and 6% (from 272 to 600 °C). The main molecules detected by MS measurements were water ($m/z = 17, 18$), carbon dioxide ($m/z = 44$) and biphenyl and its fragments ($m/z = 74, 75, 76, 77, 152, 153, 154$ and 155). According to elemental analysis data, the $Sn_2(C_{12}H_8)_1O_2(OH)_2$ formula could be proposed for the xerogel. The TGA recorded in air gave a final residue of 69.0% close to that expected from the proposed chemical formula (68.7%). The studies performed on the other xerogels led to similar conclusions. Then, the organization at the nanometer scale of the xerogels was studied by powder X-ray diffraction. The XRD pattern of $\mathbf{X_{2c}}^{120}$ showed a diffraction feature at ca. $2\theta = 4.8°$ corresponding to a distance between diffractive planes of about 1.84 nm according to the Bragg law [Fig. 3(a)]. This value was in close agreement with the one calculated from the tin–tin distance determined in the single-crystal X-ray structure of 4,4″-bis(tricyclohexylstannyl)terphenyl [Fig. 3(b)].[21] Furthermore, the xerogels obtained from **2b** and **2d** exhibited a similar feature in their powder XRD pattern (Table 2). As a matter

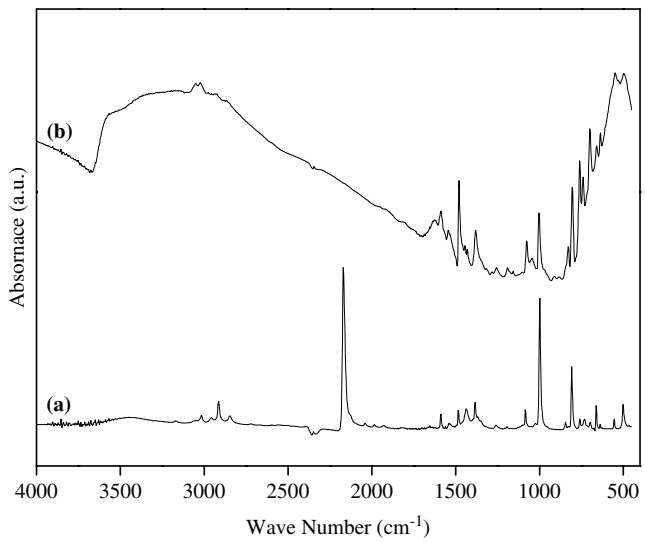

Figure 2. Infrared spectrum of (a) **2a** and (b) $\mathbf{X_{2b}}^{120}$.

Table 2. Structural data for hybrid xerogels prepared in homogeneous conditions

Sample	2θ (deg)	d_{exp} (nm)	d_{cal} (nm)	Tilt angle (deg)	Domain size[a] (nm)
$\mathbf{X_{2a}}^{120}$	6.3	1.40	1.48	19	4.2
$\mathbf{X_{2b}}^{120}$	5.7	1.55	1.54	0	3.3
$\mathbf{X_{2c}}^{120}$	4.8	1.84	1.97	21	4.8
$\mathbf{X_{2d}}^{120}$	4.3	2.05	2.05	0	4.2
$\mathbf{X_{2e}}^{120}$	—	—	—	—	—

[a] Determined from X-ray line broadening (±0.5 nm).

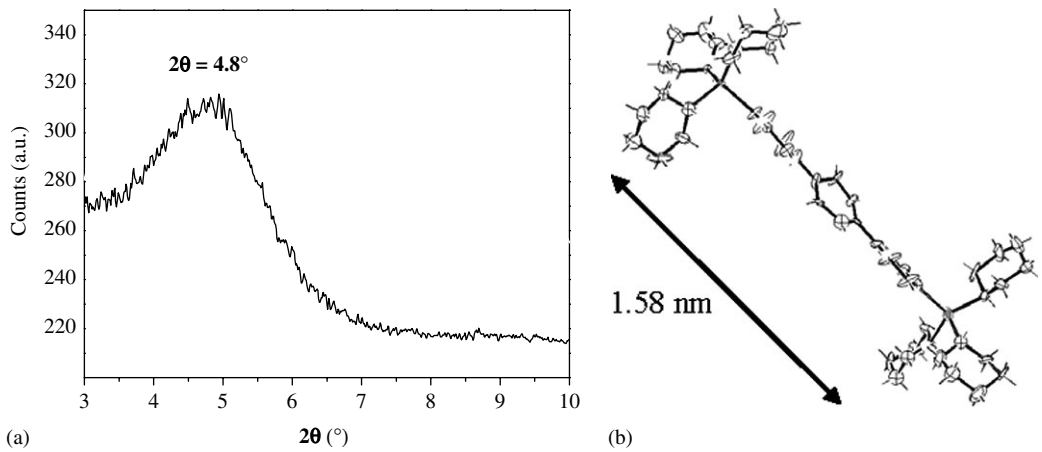

Figure 3. (a) Powder XRD of $\mathbf{X_{2c}}^{120}$; (b) X-ray crystal structure of 4,4″-bis(tricyclohexylstannyl)terphenyl.[21]

DOI: 10.1002/aoc

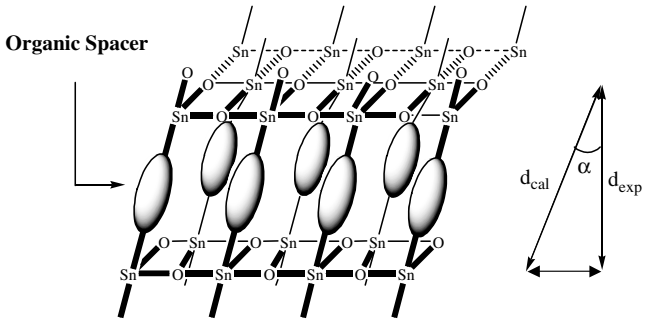

Figure 4. Schematic representation of the organization at the nanometer scale of the self-assembled tin-based hybrid materials.

of fact, for xerogels prepared from precursors including rigid and semi-rigid linkers, we have proposed a structural model in which tin oxide planes are separated by layers of self-assembled organic spacer, a tilt angle of the spacer being in some cases postulated to fit the experimental and calculated oxide plane distances (Fig. 4). Regardless the rigid or semi-rigid spacer used, the organized domain size was about 4 ± 0.5 nm according to X-ray line broadening. [The mean organized domain or particle size is given by the Scherer formula $t = (0.9 * \lambda)/\beta \cos\theta$ where λ is the wavelength, ε the angular half-width of the *hkl* peak for the studied sample and θ the Bragg angle for the chosen *hkl* reflection. See Jenkins and Synder.[29]] In contrast, such self-assembly was not observed under homogeneous hydrolysis condition from **2e**, which contained a flexible hexylene bridge. Textural properties of these hybrid xerogels were also strongly dependent upon the precursor nature. Thus, the specific surface area of $\mathbf{X_{2b}}^{120}$, which included a rigid spacer, was much lower than that measured for $\mathbf{X_{2e}}^{120}$, which contained a flexible alkyl chain (Table 3). Nonetheless, the origin of these differences remains unclear. At this stage, it is worth mentioning that microemulsion hydrolysis conditions were required to obtained self-assembled tin-based hydrid materials from precursor **2e** as previously reported for a butylene spacer.

To obtain tin dioxide materials, xerogels $\mathbf{X_{2b}}^{120}$ and $\mathbf{X_{2e}}^{120}$ were then calcined under an oxygen flow at a temperature higher than 400 °C according to the TGA measurements. The complete removal of the organic bridges was evidenced by IR spectroscopy. Whereas the dried xerogel $\mathbf{X_{2b}}^{120}$ was clearly amorphous [Fig. 5(b)], the XRD features of the annealed xerogels became progressively sharper with increasing temperature of the thermal treatment, revealing the increase in crystal size due to sintering process and particle growth [Fig. 5(c, d)]. This behavior accounted for the formation of SnO_2 cassiterite particles, the average crystallite sizes of which were estimated to be between 5 and 31 nm from the Scherer formula.[29] (Table 3). Calcination induced strong changes on the textural properties of the resulting materials. For each sample studied, the N_2 adsorption–desorption isotherm was a type IV isotherm with a type H2 hysteresis loop, which

Table 3. Textural properties and crystallinity of dried and calcined samples

Sample	S_{BET}[a] ($m^2\ g^{-1}$)	Total pore volume[a] ($cm^3\ g^{-1}$)	Mean pore diameters[a] (nm)	Mean crystallite size[c] (nm)
$\mathbf{X_{2c}}^{120}$	4	0.01	—[b]	—
$\mathbf{X_{2c}}^{400}$	62	0.09	6, 9.5	5
$\mathbf{X_{2c}}^{500}$	25	0.05	6.5, 13, 20	31
$\mathbf{X_{2e}}^{120}$	118	0.15	—[b]	—
$\mathbf{X_{2e}}^{400}$	45	0.08	8.5	12
$\mathbf{X_{2e}}^{500}$	26	0.05	—[b]	31

[a] Surface areas were determined by BET, mean pore diameters by BJH theory (adsorption branch), and pore volumes by single-point analysis. [b] BJH theory cannot be used to estimate the pore size in this case. [c] Determined from X-ray line broadening (±0.5 nm).

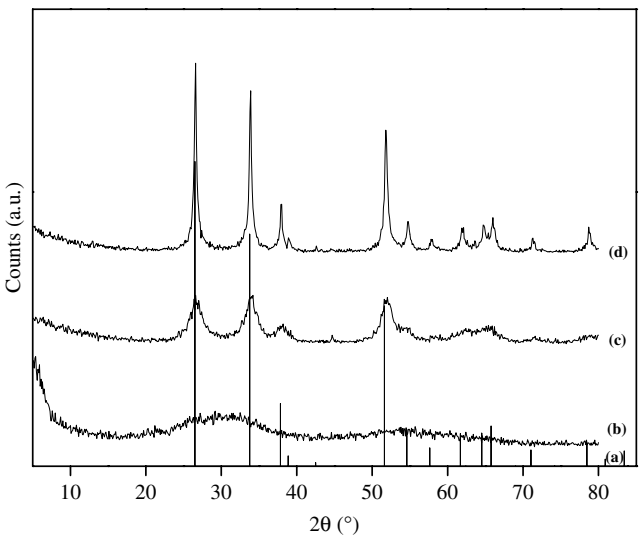

Figure 5. X-ray diffraction patterns of (a) cassiterite SnO_2 (JCPDS 41–1445), (b) $\mathbf{X_{2b}}^{120}$, (c) $\mathbf{X_{2b}}^{400}$ and (d) $\mathbf{X_{2b}}^{500}$.

was typical of mesoporous solids according to the IUPAC classification (Fig. 6).[30] However, some differences could be noted as function of the precursor nature. Thus, a strong enhancement of the BET surface areas was observed for $\mathbf{X_{2b}}^{120}$ after calcination at 400 °C, followed by a significant decrease as the temperature of the annealing treatment was increased up to 500 °C. This behavior was closely connected to the competition between two opposite processes, on one hand the formation of pores arising from the decomposition of the organic spacer and, on the other hand, the closure of the porosity and particle growth upon thermal activation. For sample prepared from $\mathbf{X_{2e}}^{120}$, a continuous decrease of the BET surface areas was evidenced as the calcination temperature was raised. Moreover, the differences in the pore size distributions were even more pronounced. Indeed, the flexible hexylene spacer led to a broad pore size distribution

DOI: 10.1002/aoc

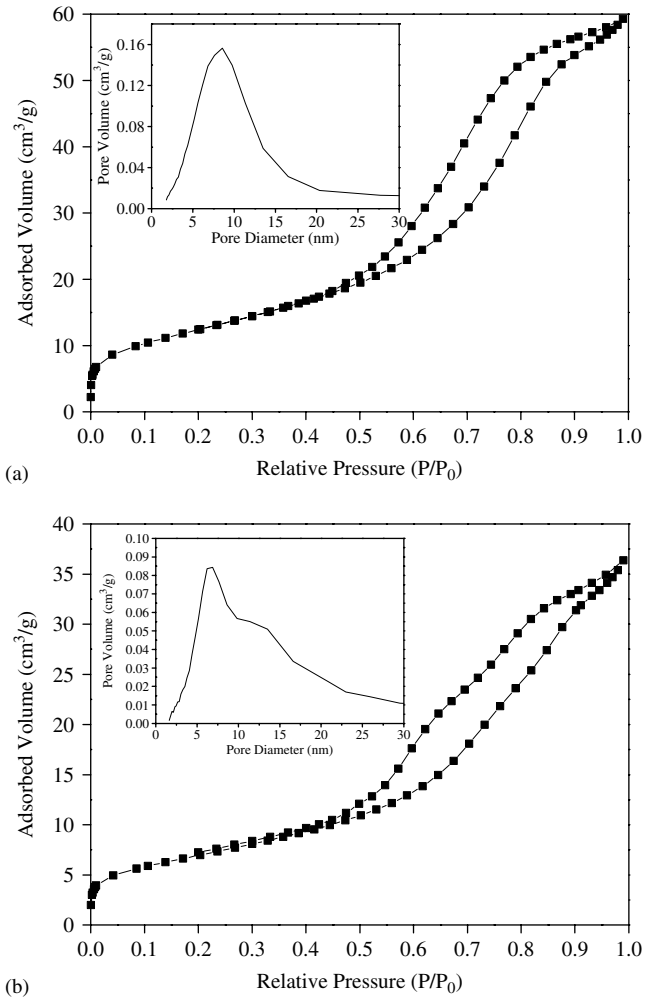

Figure 6. Nitrogen gas adsorption-desorption isotherms and BJH pore-size distribution (inset) of (a) $\mathbf{X_{2e}}^{400}$ and (b) $\mathbf{X_{2b}}^{500}$.

with, for instance, a mean pore size value of 8.5 nm for $\mathbf{X_{2e}}^{400}$. In contrast, the hysteresis loops found for $\mathbf{X_{2b}}^{400}$ and $\mathbf{X_{2b}}^{500}$ were rather unusual giving polymodal pore size distributions which might be due to different pore families (Fig. 6, Table 3). This unexpected hysteresis loop shapes could be rationalized on the basis of TEM images. Thus, the TEM image of $\mathbf{X_{2e}}^{400}$ showed that the sample was made of a porous network of aggregated nanoparticles, the size of which varied from 10 to 20 nm [Fig. 7(a)]. As a consequence, the mesoporosity detected by N_2 adsorption measurements could be attributed to the internanoparticle space as previously proposed for other SnO_2 materials prepared by sol–gel techniques.[31] By contrast, $\mathbf{X_{2b}}^{500}$ showed a more complex morphology since it contained both nanoparticles, i.e. 10–30 nm, and much larger particles, the size of which was higher than 200 nm [Fig. 7(b)]. Consequently, the polymodal pore size distributions could be related to the interparticle space existing between particles of different sizes. To some extent, the nature of the hybrid therefore influences both texture and morphology of the

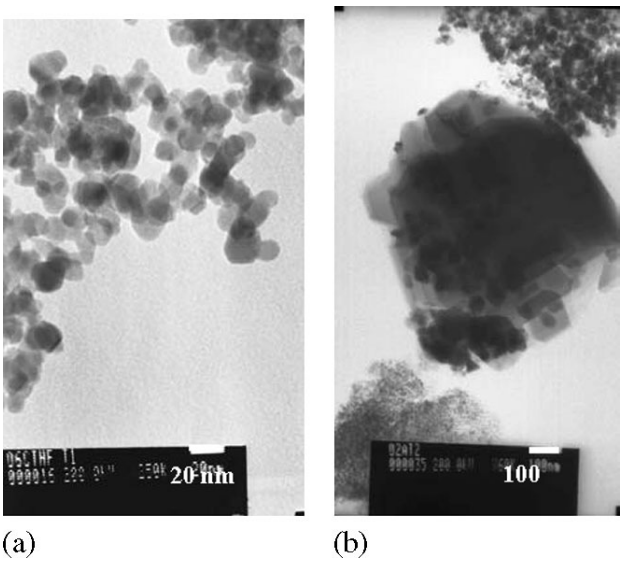

Figure 7. Transmission electron micrographs of (a) $\mathbf{X_{2e}}^{400}$ and (b) $\mathbf{X_{2b}}^{500}$.

tin dioxide materials obtained after calcination. However, treatment at 500 °C led to close BET surface area and mean crystallite size as annealing at very high temperature is known to erase completely the 'fingerprint' of the organic spacer.

Acknowledgment

The authors are indebted to Professor Rudi Willem, Professor Monique Biesemans, Dr C. Labrugère, Dr H. Allouchi, Dr Cecile Zakri, Dr Guy Campet, Dr Elisabeth Sellier and Dr Hubert Cachet for solid-state NMR, XPS, single crystal and powder X-ray diffraction, TEM and photoelectrochemical studies, respectively. Mrs Odile Babot and Marie-Claude Rascle are thanked for their valuable assistance. The Aquitaine Region (MdB fellowship), the Centre National de la Recherche Scientifique (Material Program Grant) and the European Community (FAME Network of Excellence) are acknowledged for partial support of this work.

REFERENCES

1. Gomez-Romero P, Sanchez C (eds). *Functional Hybrid Materials.* Wiley-VCH: Weinheim, 2003.
2. Loy DA, Shea KJ. *Chem. Rev.* 1995; **95**: 1431.
3. Sanchez C, Soler-Illia GJAA, Ribot F, Mayer C, Cabuil V, Lalot T. *Chem. Mater.* 2001; **13**: 3061.
4. Soler-Illia GJAA, Sanchez C, Lebeau B, Patarin J. *Chem. Rev.* 2002; **102**: 4093.
5. Sanchez C, Arribart H, Giraud Guille MM. *Nat. Mater.* 2005; **2**: 277.
6. Sagiv J. *J. Am. Chem. Soc.* 1980; **102**: 92.
7. Inagaki S, Guan S, Fukushima Y, Ohsuna T, Terasaki O. *J. Am. Chem. Soc.* 1999; **121**: 9611.
8. Melde BJ, Hollande B, Blanford CF, Stein A. *Chem. Mater.* 1999; **11**: 3302.
9. Asefa T, MacLachlan MJ, Coombs N, Ozin GA. *Nature* 1999; **402**: 867.

10. Moreau JJE, Vellutini L, Bantignies J-L, Wong Chi Man M, Bied C, Dieudonné P, Sauvajol J-L. *J. Am. Chem. Soc.* 2001; **123**: 7957.
11. Tillman N, Ulman A, Schildkraut JS, Penner TL. *J. Am. Chem. Soc.* 1988; **110**: 6136.
12. Fadeev AY, Mc Carthy T. *J. Am. Chem. Soc.* 1999; **121**: 12184.
13. Shimada T, Aoki K, Shimoda Y, Nakamura T, Tokunaga N, Inagaki S, Hayashi S. *J. Am. Chem. Soc.* 2003; **125**: 4688.
14. Yoshino N, Yamamoto Y, Hamano K, Kawase T. *Bull. Chem. Soc. Jpn* 1993; **66**: 1754.
15. Perrot H, Jaffrezic-Renault N, Clechet P. *J. Electrochem. Soc.* 1990; **137**: 598.
16. Ribot F, Lafuma A, Eychenne-Baron C, Sanchez C. *Adv. Mater.* 2002; **14**: 1496.
17. Ribot F, Veautier D, Guillaudeu SJ, Lalot T. *J. Mater. Chem.* 2005; **15**: 3973.
18. Vilaça G, Barathieu K, Jousseaume B, Toupance T, Allouchi H. *Organometallics* 2003; **22**: 4584.
19. Boutet S, Jousseaume B, Biesemans M, Willem R, Labrugère C, Delattre L. *Chem. Mater.* 2005; **17**: 1803.
20. Jousseaume B, Riague H, Toupance T, Lahcini M, Mountford P, Tyrell BR. *Organometallics* 2002; **21**: 4590.
21. Elhamzaoui H, Jousseaume B, Toupance T, Allouchi H. *Organometallics* (in press).
22. Vilaça G, Jousseaume B, Mahieux C, Toupance T, Belin C, Cachet H, Bernard M-C, Vivier V. *Adv. Mater.* 2006; **18**: 1073.
23. El Hamzaoui H, Jousseaume B, Riague H, Toupance T, Dieudonné P, Zakri C, Maugey M, Allouchi H. *J. Am. Chem. Soc.* 2004; **126**: 8130.
24. Elhamzaoui H, Jousseaume B, Toupance T, Zakri C, Biesemans M, Willem R, Allouchi H. *Chem. Commun.* 2006; 1306.
25. Elhamzaoui H, Toupance T, Maugey M, Zakri C, Jousseaume B. *Langmuir* 2007; **23**: 785.
26. Barrett EP, Joyner L, Halenda PP. *J. Am. Chem. Soc.* 1951; **73**: 373.
27. Cachet H, Vivier V, Toupance T. *J. Electroanal. Chem.* 2004; **572**: 249.
28. Kay A, Grätzel M. *Chem. Mater.* 2002; **14**: 2930.
29. Jenkins R, Synder RL. *Introduction to X-ray Powder Diffractometry*. Wiley: New-York, 1996.
30. Sing KSW, Everett DH, Haul RAW, Moscou L, Pierotti RA, Rouquerol J, Siemieniewska T. *Pure Appl. Chem.* 1985; **57**: 603.
31. Toupance T, Babot O, Jousseaume B, Vilaça G. *Chem. Mater.* 2003; **15**: 4691.

DOI: 10.1002/aoc